Trade-offs between lens complexity and real estate utilization in a free-space multichip global interconnection module

Predrag Milojkovic*

Applied Photonics, 4031 University Drive, Suite 200, Fairfax, Virginia 22030

Marc P. Christensen

Southern Methodist University, Department of Electrical Engineering, School of Engineering, Dallas, Texas 75275

Michael W. Haney

University of Delaware, Electrical and Computer Engineering Department, Evans Hall, Newark, Delaware 19716

Received August 26, 2005; revised December 14, 2005; accepted December 16, 2005; posted January 26, 2006 (Doc. ID 64394)

The FAST-Net (Free-space Accelerator for Switching Terabit Networks) concept uses an array of wide-field-of-view imaging lenses to realize a high-density shuffle interconnect pattern across an array of smart-pixel integrated circuits. To simplify the optics we evaluated the efficiency gained in replacing spherical surfaces with aspherical surfaces by exploiting the large disparity between narrow vertical cavity surface emitting laser (VCSEL) beams and the wide field of view of the imaging optics. We then analyzed trade-offs between lens complexity and chip real estate utilization and determined that there exists an optimal numerical aperture for VCSELs that maximizes their area density. The results provide a general framework for the design of wide-field-of-view free-space interconnection systems that incorporate high-density VCSEL arrays. © 2006 Optical Society of America

OCIS codes: 200.4650, 080.1010, 200.2610.

1. INTRODUCTION

Systems that use smart pixel-based free-space optical interconnections (FSOI) are intended to eliminate the bottlenecks associated with planar electronic interconnection technologies. The FAST-Net (Free-space Accelerator for Switching Terabit Networks) concept achieves a global interconnection pattern across many chips distributed across a single plane.[1] The prototype system incorporates two-dimensional (2D) arrays of monolithically integrated vertical cavity surface emitting lasers (VCSELs) and photodetectors (PDs) that are bumpbonded to complementary metal-oxide semiconductor, application-specific integrated circuits (ASICs) that provide the data processing functions of the smart pixel.[2] The feature size and density of the multichip VCSEL/PD arrays lead to registration and resolution accuracy requirements that are of the order of tens of micrometers across the entire multichip substrate. Previous prototypes of this system successfully used an array of seven-element, commercial off-the-shelf (COTS) lenses to effect the high-density global multichip interconnection pattern. Although successful, this seven-element design was not optimized for the FAST-Net performance criteria and introduced high transmission loss. This highlighted the need for methods that minimize lens loss and achieve the most efficient optical design for this system (i.e., minimum number of optical surfaces). This goal could be achieved with aspherical surfaces in the multielement FAST-Net lenses, so it is of considerable interest to determine the gain in efficiency that would result from such substitution.

Another important and related area for analysis is the trade-off that exists between chip space utilization (i.e., area density of the VCSEL array) and lens complexity. The trend in VCSEL development is toward lower threshold currents to achieve lower overall power dissipation, which implies smaller current apertures and therefore larger beam divergence. With larger beam divergence, however, it becomes necessary in the FAST-Net system to employ microlenses above VCSELs to reduce their divergence. Such use of microlenses makes it possible to collect most of the VCSEL light while keeping the imaging optics relatively simple by lowering the effective numerical aperture (NA) of VCSELs. However, because of their size and integration approaches, microlenses introduce an additional limit on the area density of VCSELs that can be worse than the limit imposed by heat dissipation. Therefore, there are a number of trade-offs in the system that need to be explored to achieve an overall optimum design.

There are a number of earlier papers that address scaling issues and performance trade-offs in FSOI systems.[3–7] Although this field has been extensively analyzed, to our knowledge none of the previous work has looked at the tradeoffs that exist among real estate utilization, thermal considerations, and optical complexity in such systems. In this paper we address these issues and analyze how they affect performance of the FAST-Net type of system.

1084-7529/06/071787-9/$15.00

Section 2 provides a description of the FAST-Net approach and highlights its unique features and optical performance requirements. The general approach to minimizing the number of optical surfaces by using aspherical elements is provided in Subsection 3.A, and its application to FAST-Net is given in Subsection 3.B. General trade-offs between lens complexity and space utilization are analyzed in Section 4. This new design and analysis framework and its key results are summarized in Section 5.

2. FAST-NET OPTICAL SYSTEM

Figure 1 depicts a canonical FAST-Net system. Its interconnection part comprises a set of identical lenses in a 2D array and a mirror. Beneath the lenses is an array of matching smart-pixel chips with associated arrays of optoelectronic elements (VCSELs and PDs) that are grouped in clusters on each chip. This clustering and the position of each lens allow the system to effect a global bidirectional shuffle interconnection pattern between sources and detectors.[1] Typical parameters of a system are: VCSEL circular active area diameter of $\sim 10\ \mu$m; square photodetectors that are 50 μm on a side; 16 chips that need to be interconnected, and the corresponding 16 clusters of interleaved VCSELs and detectors on each chip. Each VCSEL/detector cluster has a number of optoelectronic elements distributed on a grid. A cross section of the unfolded system with the associated interconnection pattern is shown in Fig. 2 (only VCSELs are shown on the left side and only corresponding detectors on the right side). VCSELs are considered to be telecentric sources as they emit perpendicularly to the chip surface, and the chief ray of each VCSEL beam is parallel to the optical axis of the corresponding lens. The VCSEL arrays are located at the focal plane of the lens, so their respective offset from the optical axis determines the tilt angle of the beam that exists the lens. An f/1 lens design is desired because it would provide a steep beam angle and minimize the length of the system,[4] providing an approximately cubic-shaped structure for an unfolded system, as depicted in Fig. 2. In the FAST-Net system, each lens serves simultaneously as the transmitting and receiving element. Pairs of lenses implement an imaging system between associated clusters of input/output devices on the chip beneath the lenses. Each lens provides for a number of simultaneous optical links between its chip and every other chip in the common plane. As can be seen in Fig. 2, lens 1 provides optical links from chip A to chips A, B, C, and D using lens pairs 1-1, 1-2, 1-3, and 1-4. Therefore, a single lens in the system must capture light from all VCSELs beneath it, distribute the light over all lenses in the system (using the mirror to fold the system back on itself), and also simultaneously receive light beams that are coming from VCSELs under other lenses and focus them on the corresponding detectors beneath. This bidirectional aspect and simultaneous, multiple, pairwise lens operation are distinguishing features of the FAST-Net optical system.

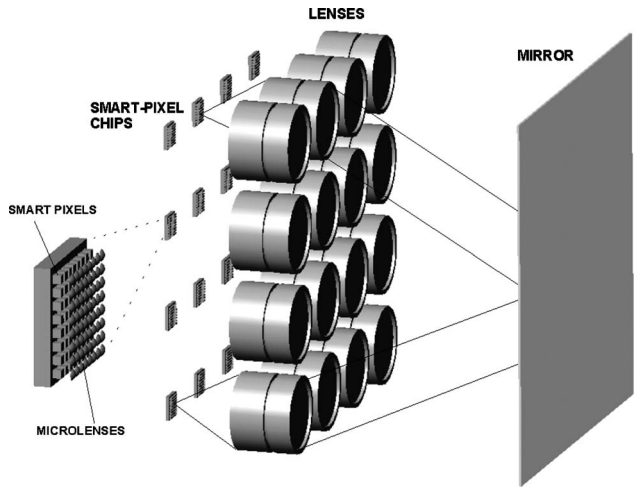

Fig. 1. In the FAST-Net system, a multichip smart pixel array is linked to itself in a global optical interconnection pattern provided by the lens array and the mirror. An optical beam shown depicts the light path between a VCSEL on one of the smart-pixel chips and the corresponding photodetector on another chip.

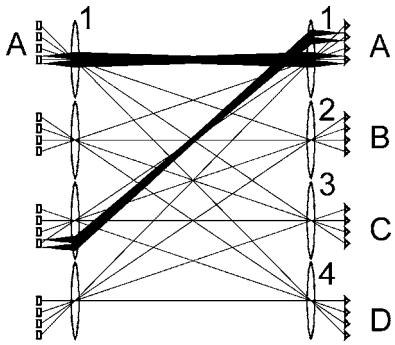

Fig. 2. Schematic cross section of the FAST-Net system showing interconnection pattern between smart-pixel chips. The position of each VCSEL is mapped onto the corresponding beam angle in the space between sending and receiving lenses. After passing through the receiving lens the angle of the beam is mapped back into the position of the focused spot on the receiving chip.

Previous prototypes of this system successfully used an array of seven-element (13 spherical surfaces), COTS lenses to provide the high-density global multichip interconnection pattern. Although successful, this seven-element design was not optimized for the FAST-Net performance criteria. Measurements on the first prototype of the FAST-Net system showed that the COTS lens introduced a transmission loss of 32% at 850 nm.[1] Since a channel in the FAST-Net system comprised two lenses, there was an approximately 50% light loss per channel introduced by lenses alone. Antireflective coating of all optical surfaces of a lens could minimize the reflection loss. However, an additional benefit would be derived if the number of lens elements could be minimized to lower the overall lens loss (comprising reflection, absorption, and scattering losses) and simultaneously simplify its mechanical design and alignment. Since an aspherical surface has a larger number of degrees of freedom than a spherical surface has, it should be possible to replace spherical surfaces with a smaller number of aspherical surfaces and keep the same quality of imaging. In mass production, modern manufacturing techniques can provide aspherical surfaces at competitive costs, so the goal here would be to achieve reasonable overall cost through the use of asperical surfaces and the resulting reduced number of elements in the imaging lenses.

To determine the benefits of this replacement one needs to determine how many spherical surfaces could be replaced with one aspheric surface for a given system. A framework for such analysis based on the degrees of freedom an optical system has available to correct aberrations was developed by Schulz,[8] and his approach will be applied to the FAST-Net system.

3. REPLACEMENT EFFICIENCY OF AN OPTICAL SYSTEM

A. Replacement Efficiency for Optical Designs

The general problem of calculating how efficiently spherical surfaces could be replaced by asphericals in any rotationally symmetric optical system was solved by Schulz.[8] To express the advantage of this replacement he introduced the replacement efficiency parameter R, defined as the ratio of the number of spherical surfaces to the equivalent number of aspherical surfaces needed to achieve the same quality of imaging. His approach was based on the notion that an aspherical surface has a higher number of degrees of freedom than a spherical surface, and therefore could be used more efficiently in controlling aberrations of optical systems, thus minimizing the number of optical elements. To quantify this approach Schulz analyzed the wave aberration polynomial W for a rotationally symmetric optical system[8]:

$$W(r,\rho,\cos\theta)=\sum_{\mu}\sum_{\nu}\sum_{\tau}{}_{\mu}C_{\nu\tau}r^{\mu}\rho^{\nu}\cos^{\tau}\theta, \tag{1}$$

where r and ρ are fractional angular measures of the field and aperture points, respectively, and θ is the angle between them. Subscripts μ, ν, and τ have to satisfy certain constraints that follow from rotational symmetry. Aberration coefficients ${}_{\mu}C_{\nu\tau}$ can be graphically represented as the circles shown in Figs. 3 and 4, where the number in a circle represents index τ, and the position of each coefficient is determined by its indices μ and ν. In this representation, for example, third-order aberration coefficients (the five Seidel aberrations) are on the line connecting $\mu=\nu=4$, and nine fifth-order aberration coefficients are on the line connecting $\mu=\nu=6$. If an optical system comprises spherical surfaces, then their curvatures, or both their curvatures and positions, could be used to control coefficients ${}_{\mu}C_{\nu\tau}$. Schulz analyzed both cases and gave formulas for calculating the required number of spherical surfaces.

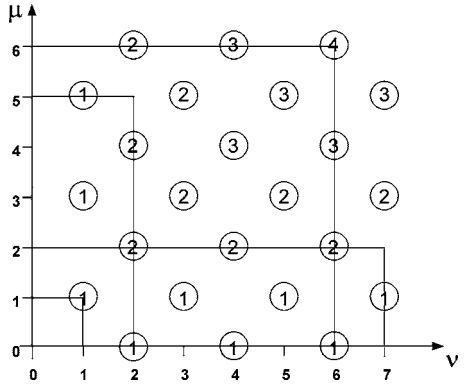

Fig. 3. Graphical representation of the terms of the wave aberration function. Large and small squares and rectangles encompass the coefficients, which are relevant for the typical imaging cases listed in Table 1.

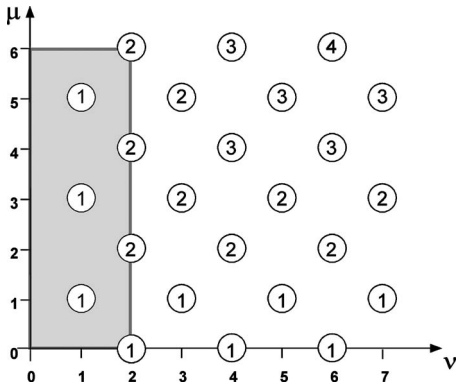

Fig. 4. Rectangle that covers all relevant aberration coefficients for the analyzed FAST-Net system. The aspect ratio of the rectangle depends on the angular imbalance ratio of the system (ratio of the maximum field and aperture angles).

The FAST-Net optical system has a large number of off-axis lens pairs that are not rotationally symmetric. However, since lenses in the FAST-Net system operate at infinite conjugate ratio we may analyze the performance requirement of a single lens only and disregard the manner in which it is connected to other lenses. Because each lens is itself rotationally symmetric, we can apply the theory for the general rotationally symmetric optical system to it.

The aberration polynomial can also be expressed as a series (double summation) of a function of one variable (r, ρ or θ) that itself is a summation over index μ, or over ν, or over τ. The form that is convenient to FAST-Net is a series expansion of polynomials in variable r (summation over index μ):

$$W=\sum_{\nu}\sum_{\tau}G_{\nu\tau}(r)\rho^{\nu}\cos^{\tau}\theta, \qquad G_{\nu\tau}(r)=\sum_{\mu}{}_{\mu}C_{\nu\tau}r^{\mu}, \tag{2}$$

where $G_{\nu\tau}$ represents a function whose coefficients could be controlled by shape coefficients of an aspheric surface of the form given in

$$z=\frac{a_1h^2}{1+\sqrt{1-a_1^2h^2}}+a_2h^4+a_3h^6+\cdots \tag{3}$$

In this formula, z is the sag of the aspherical surface, h is the radial distance of a point on the aspheric surface from the optical axis, and $a_1,a_2,\ldots,a_n$, are its shape coefficients. Schulz noted that it would be possible to use shape coefficients of aspherical surfaces to control ${}_{\mu}C_{\nu\tau}$ coefficients of aberration polynomial with fewer surfaces than in the all-spherical case. The required quality of imaging limits the set of aberration coefficients that need to be controlled, and it is possible to determine the number of spherical surfaces and minimum number of asphericals that could control them. Their ratio would give the replacement efficiency parameter R of the system.

As already mentioned, either we could use the shape parameter of a surface to control a single aberration term, or we could use both shape parameter and position of a surface to control two aberration terms. The first case is

easier to analyze because shape parameters for either spherical (curvature) or aspherical surfaces directly map onto a set of aberration coefficients, and it is possible to derive formulas for the number of spherical and equivalent aspherical surfaces. The second case is more realistic but also more complicated to calculate in the case of aspherical surfaces: variable distances between aspherical surfaces can be used to control some aberration coefficients and (1) reduce the required degree of an aspheric, (2) transform an aspherical into a spherical surface, or (3) completely eliminate aspherical surface(s). The exact aberration control achieved in this case depends on the number of aspherics and the number and distribution of their respective coefficients. There is no closed-form expression for the number of surfaces in this case; one must count surfaces and their respective shape factors and determine the overall minimum number of aspherics. We adopted this approach for the FAST-Net analysis because it is more realistic.

Table 1 shows four typical imaging cases separated by the relative ratio of the aperture and field angles. It can be shown[9] that when both angles are similar in magnitude (either large or small, i.e., aberration coefficients are within the small or large squares in Fig. 3), then the replacement efficiency is relatively low. On the other hand, the more different the values of the field and aperture angles, the more efficient replacement is possible. Fourtunately, the FAST-Net system is in the latter category, so it should be possible efficiently to replace its optical spherical surfaces with aspherical ones.

B. Application of the Efficiency Theory to the FAST-Net System

As stated above, Eq. (2) lends itself to the analysis of the FAST-Net optical system since it is appropriate for describing the aberration function of narrow beams in wide-field-of-view systems. However, in order to apply this approach it is necessary to determine the aspect ratio and size of the rectangle that covers all relevant aberration coefficients for the FAST-Net (Figs. 3 and 4).

Simple geometrical analysis of the system, with the assumption that it uses f/1 optics, provides the maximum field half-angle of 26.5° for the lenses in the FAST-Net system. VCSELs are assumed to have a NA of 0.1, meaning that the angular extent of the VCSEL cone of light (angular measure of aperture) is ~6° half-width. The ratio of these two angles determines the ratio of maximum degrees of expansion in μ and ν. This *angular imbalance ratio* is an important parameter for the analysis that follows. From the angles for the f/1 system, it is easy to see that the angular imbalance is ~4. Since the analyzed system has a smaller angular field (~18°, because the clusters do not fill the whole lens to accommodate for possible beam clipping at the lens edge), the angular imbalance is ~3. Therefore the part of the $\mu-\nu$ plane that is important in this case can be represented by a rectangle whose μ dimension is 3 times its ν dimension.

Table 1. Replacement Efficiency Parameter *R* for the Typical Imaging Cases Separated by the Field and Aperture Angles

Field Angle (μ)	Aperture Angle (ν)	
	Small	Large
Small	*R* small (Gaussian optics)	*R* high (aplanatic imaging, e.g., microscope objective)
Large	*R* high (FAST-Net)	*R* small (wide angle wide aperture lenses)

Schulz outlined the procedure for determining the required number of aspherical surfaces as a function of maximum μ, ν, and τ by overlaying lines in the $\mu-\nu$ plane.[8] The lines correspond to individual aspherical surfaces and their lengths provide the complexity of the surface (number of aspherical coefficients). If we want to use the minimum number of lines to cover this rectangle (each line represents one aspherical surface, and we want to use the minimum number of surfaces) we need to use a line for each value of ν, because ν is smaller than μ. This leads to the form for W given as a summation of G functions over parameter ν, where each G function is a summation over μ [Eq. (2)]. From the formula for W we can see that all possible values for parameters ν and τ determine the number of different aspherical surfaces needed, while allowed values of μ determine the degree of each aspherical surface. Since an aspherical surface is a function of one variable, changing its shape parameters $(a_1,a_2,a_3,\ldots,a_n)$ will control coefficients ${}_{\mu}C_{\nu\tau}$ of the corresponding G function.

Schulz's approach is valid for determining the relative benefits of aspherics versus spherical surfaces but not for determining absolute numbers of surfaces for specific imaging conditions. Therefore, the angular imbalance ratio specifies only the aspect ratio of the rectangle used to cover the relevant part of the $\mu-\nu$ plane, while the absolute size of the rectangle should be determined by the desired optical performance of the system (i.e., the number of aberrations to control—the number of spherical surfaces needed). Ray tracing analysis of the FAST-Net system with COTS lenses using OSLO optical design software[10] was done in order to determine the absolute dimensions of the rectangle in this case. Since the size of the rectangle depends on the desired quality of imaging, the imaging goal was to get 90% of VCSEL rays onto the 50-μm-side detector. Since in the analyzed range of system parameters, detectors are at least 100 μm apart (which can be determined from Fig. 6, below, with the understanding that VCSELs and detectors have the same spacing), cross talk between adjacent detectors was not taken into consideration as it would be negligible if the imaging goal were met.

The ray-trace simulation, which used spherical surfaces with adjustable positions, determined a candidate solution that met the performance criteria with six surfaces, but was unable to determine a solution with five surfaces.[11] While it is not possible to prove such a solution does not exist, a six-surface solution was used to bound the performance. That implied that at most 12 coefficients ${}_{\mu}C_{\nu\tau}$ would have to be controlled. Based on this it was pos-

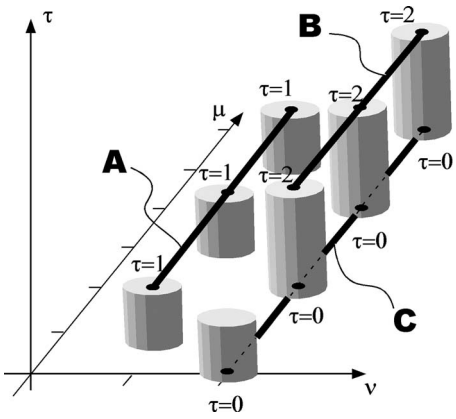

Fig. 5. Three-dimensional view of the terms of the wave aberration function that need to be controlled by aspherical surfaces in the FAST-Net system and the line segments needed to cover them.

Table 2. Wavefront Aberration Coefficients to be Controlled in the Analyzed FAST-Net System

Segment		
A	B	C
${}_1C_{11}$	${}_2C_{22}$	${}_0C_{20}$
${}_3C_{11}$	${}_4C_{22}$	${}_2C_{20}$
${}_5C_{11}$	${}_6C_{22}$	${}_4C_{20}$
		${}_6C_{20}$

sible to determine the absolute size of the rectangle. This was done by overlaying vertical rectangles of various sizes onto the diagram of Fig. 4, each with the same aspect ratio of 3, and counting the sum of the numbers in the encompassed circles (i.e., the number of coefficients ${}_\mu C_{\nu\tau}$). The sum closest to but $\leqslant 12$ was determined to be inside the rectangle with sides $\mu_{max}=6$ and $\nu_{max}=2$. It was 10 (shaded rectangle in Fig. 4). Had the next-larger rectangle been used, the lens would have required many more than 12 surfaces, whereas had the next-smaller rectangle been used, the lens would have required many fewer than 12 surfaces. The fact that 10 instead of 12 coefficients were used in the analysis should not affect the final result—it can be shown that replacement efficiency parameter R is a relatively weak function of the number of spherical surfaces in a system.[8]

To determine the equivalent number of aspherical surfaces, the shaded rectangle of Fig. 4 was used. To determine the *minimum* number of aspherical surfaces, it is necessary to cover the rectangle with the smallest possible number of lines, which implies in turn the use of vertical lines. The numbers inside circles (the *number* of τ values) can be considered to be the heights of the circular "pins" protruding from the plane of paper. To give the spatial impression, Fig. 5 shows a three-dimensional (3D) view of the shaded rectangle: The minimum number of line segments sufficient to cover all "pins" for all values of τ is 3. Segments have the form given in Eq. (2). For example, the C segment is an aspherical surface given as the summation over μ (from 0 to 6) with $\nu=2$ and $\tau=0$. Since there are four "pins" covered by the C segment, that segment (i.e., aspherical surface) can control four wave aberration coefficients. The aberration coefficients that can be controlled with all three segments A, B, and C are given in Table 2. Each column in Table 2 represents a single aspherical surface with the number of aspheric coefficients equal to the number of rows in the column.

The replacement efficiency parameter R can now be determined for both fixed surface position and variable position cases. If we consider surfaces to be positionally fixed, then theoretically we can replace ten spherical surfaces with three aspherical surfaces, giving $R=3.3$. If we give each spherical and aspherical surface one more degree of freedom (its position) then it should be possible to replace five spherical with two aspherical surfaces and one spherical surface. This reduction in the number of aspherical surfaces follows from the observation that three aspherical surfaces have two intersurface distances, which can be used to control two out of three aspherical coefficients of either A or B aspherics (Table 2) leaving only one coefficient to be controlled, which can be done by a single spherical surface. This approach then results in $R\approx 2$, and we will consider this to be the replacement efficiency available in the FAST-Net system with given parameters. We take this to be the final result because it was derived under the more realistic assumption of exerting control over both curvatures and positions of lens surfaces—degrees of freedom that certainly exist in practical lens design and layout.

To validate the accuracy of this approach a lens file was constructed in OSLO in which the lens had three aspherical surfaces and each surface had the appropriate number of shape parameters (3, 4, and 3).[11] Two aspherical surfaces were cemented together, which could pose a practical difficulty for lens manufacturing, but it did not affect the theoretical results. The lens was then optimized and it achieved slightly better imaging results for the FAST-Net system than the one with six spherical surfaces. Then a lens with two aspherics was tried, but it could not achieve the target performance. Therefore, the ray-trace simulation confirmed (within the accuracy of the optimization techniques) that, for the case analyzed, the efficiency $R\sim 2$.

This result, derived for a specific FAST-Net system, suggests that it should be possible to efficiently (by approximately the factor of 2) reduce the number of spherical surfaces in such a system by replacing them with aspherical surfaces. This benefit comes from the fact that the field angle and aperture angle in the FAST-Net system are disparate; for the system examined, the disparity was of the order of 3. However, if the VCSELs had larger NA, that benefit would start to disappear. Such ramifications are discussed in Section 4.

4. TRADE-OFFS BETWEEN REAL ESTATE UTILIZATION AND LENS COMPLEXITY IN VCSEL-BASED INTERCONNECTION SYSTEMS

One of the goals of VCSEL research is the reduction of the threshold current, which improves overall laser efficiency.[12,13] Since it is necessary to achieve critical current density for lasing, smaller threshold current means a smaller active aperture of a device, which leads to larger

divergence angles of VCSEL beams. Opposing trends emerge in FAST-Net systems. VCSELs may have smaller apertures (and therefore lower power dissipation) in order to pack as many of them as possible onto the chip and maximize real estate utilization and efficiency. At the same time, their divergence angles would be larger, and their NA might reach 0.4 or more. Larger NA would require a larger number of optical surfaces in the system and would reduce the angular imbalance ratio of the optical system, which would in turn reduce replacement efficiency. Both effects would lead to more complex optical systems than would be necessary otherwise. In other words, optimizing the VCSEL arrays without regard to the remainder of the system can have a deleterious effect. One remedy might be to use microlenses above VCSELs in order to lower their apparent NA and improve replacement efficiency. However, this has the drawback that VCSEL area density would be limited by the spacing of the microlenses, which might have diameters of the order of hundreds of micrometers and would position VCSELs farther away than cooling capabilities would require.

An example of the trends just described is provided by a further evolution of the FAST-Net system that involves much denser and larger arrays of optoelectronic elements and custom-designed lenses. This system, called VIVACE (VCSEL-Based Interconnects in VLSI Architectures for Computational Enhancement), uses oxide-confined low-threshold VCSELs with NA $\approx$0.26 (beam half-angle of 15°). The lenses in this system implement a multiscale approach[14] that uses micro, mini, and macrolenses simultaneously to achieve diffraction-limited and almost distortionless imaging of arrays of VCSEL and photodetector clusters across a $\sim$10 cm multichip module. The effective f/number of the compound mini–macrolens is $\sim$1.1, and the field angle is close to 26°. Since the VCSEL NA is quite high, the angular imbalance ratio would be low, which would result in low replacement efficiency for this system. However, the microlenses lower the apparent NA of VCSELs to $\sim$3° half-angle, which in turn results in an increased replacement efficiency and therefore a simpler lens design.

It would be useful from the system design viewpoint to develop a framework for the analysis of the trade-offs between real estate utilization and optical complexity, as it might help system designers to utilize resources optimally. In order to do that a number of assumptions will be made. These assumptions amount to using a very simplified model for VCSEL operation and disregarding second-order effects. In addition, lens complexity results from Section 3 will be used in this section—they were derived for the specific system that was analyzed there, but are representative of general trends. In other words, we are laying the groundwork for the analysis of trade-offs in these systems, but each individual case will have to be analyzed separately if specific numerical results are of interest.

Passive air cooling limits heat dissipation from the VCSEL array to around 10 W/cm^2,[15,16] and if for example each VCSEL dissipates 1 mW of heat, then there could be at most 10,000 VCSELs/cm^2 on a chip. In other words, it would be possible to put a 100×100 VCSEL array in an area of 1 cm^2, and the minimum VCSEL spacing would be 100 μm. This spacing is the lower limit imposed by heat removal concerns and it can be reduced as the technology improves and VCSELs become more efficient in converting current into light, or by application of active cooling, which can push the cooling limit up to 30 W/cm^2 or even higher.[17,18] This density limit exists in all VCSEL arrays regardless of the use of microlenses.

Another limit on VCSEL spacing is imposed by the use of microlenses and their associated mechanical support structure called superstrate, which is a thin layer of glass that enhances mechanical stability of the GaAs chip.[19] The top surface of the superstrate is customarily used for microlens attachment. If the thickness of the glass superstrate is for example 300 μm (as it is in the VIVACE system) then it is possible to calculate the corresponding VCSEL spacing and the associated power dissipation per square centimeters as a function of VCSEL NA. This density limit is the result of the optical requirements of the system, because the required minimum spacing of the microlenses now limits the density of VCSEL arrays (microlens spacing and VCSEL NA are related to the thickness and index of refraction of the superstrate by the requirement that adjacent VCSEL light cones not overlap at the microlens plane). That VCSEL spacing is determined by the microlens spacing *and* by the cooling requirements significantly influences the behavior of the system with superstrate-based microlenses.

For the purpose of the dissipation analysis, we can separate the heat generated by a single VCSEL into two parts. One, which can be called static or quiescent power dissipation, is due to the VCSEL being biased at the threshold to enable fast on/off switching. At this bias level no light is generated by a VCSEL (in this idealized model), and all dissipated power is in the form of heat. The other part of dissipation, which may be called dynamic, is caused by VCSEL operation above the threshold during transmission of digital data. Part of the input power (for logical level 1) is converted into light, which the VCSEL emits, and the rest is transformed into heat.

The assumptions for the calculation of the quiescently generated heat will be that the VCSEL NA depends inversely on the diameter of the VCSEL active area, that threshold current *density* for all NAs is approximately constant,[20–22] and that VCSEL operating voltage is also constant.[21] It is then straightforward to show that the ratio of heat dissipation at threshold for various sized VCSELs is proportional to the square of the inverse ratio of their NAs. As a result, it is possible to calculate the dissipated heat at threshold for every NA by using a VCSEL with NA in air of 0.2 and threshold heat dissipation of 2 mW as a baseline (I_{thre}=1 mA, V_{thre}=2 V).[23]

However, dynamic dissipation should be added to this static dissipation to get the total generated heat. To determine the amount of this additional heat we need to estimate the VCSEL light power needed to trigger reliably the corresponding optoreceiver. Experimental results suggest that in the FAST-Net system $\sim$250 μW of optical power at the photodetector is enough for reliable detection of high-speed digital signals ($\sim$1.8 gigabits per second).[24] The worst-case light loss through the VIVACE interconnect optics is $\sim$50% so a VCSEL needs to output 500 μW of optical power. Using the typical VCSEL slope

Table 3. Parameters of the FAST-Net System for VCSELs with Different NAs

VCSEL NA	VCSEL Total Power Dissipation [mW]	VCSEL Spacing Based on Thermal Limit of 10 W/cm^2 [μm]	VCSEL Spacing for Superstrate Thickness of 300 μm [μm]	Number of Lens Surfaces
0.10	8.75	296	40	10
0.15	4.31	207	60	15
0.20	2.75	166	81	24
0.25	2.03	142	101	30
0.30	1.64	128	122	40
0.35	1.40	118	144	46
0.40	1.25	112	166	56

efficiency of 50% the modulation current needed to achieve this level of optical power would be 1 mA, so the increase in dissipation (for the idealized case of a constant voltage drop of 2 V across a typical 850 nm VCSEL) would be 1.5 mW. If the transmitted data signal is DC balanced (50% average VCSEL duty cycle) this extra heat dissipation drops to 750 μW. This power needs to be added to the threshold dissipation, and the result is the total VCSEL power dissipation that is transformed into heat. (Here we disregard the heat generated by associated electronic circuits, i.e., in the ASIC to which the GaAs chip containing VCSELs and photodetectors is bump bonded).

Under these assumptions, we determined the VCSEL spacing as a function of the VCSEL's numerical aperture for the case with microlenses and without them. The number of spherical surfaces was estimated using the results of Subsection 3.B. Results of these calculations are given in Table 3 and are graphically presented in Figs. 6–8.

Figure 6 shows the case without microlenses and illustrates that VCSEL spacing becomes smaller as VCSEL NA grows (VCSEL dissipates less heat). Lens complexity grows because higher NA means higher VCSEL beam divergence (and wider rectangle on Figure 4), implying that a larger number of spherical surfaces is needed to keep the same quality of imaging.

Figure 7 shows the case when microlenses are attached to the superstrate. One beneficial side effect of superstrate use is lowering of the VCSEL beam divergence in glass by a factor proportional to its index of refraction (assumed here to be 1.5), which helps achieve somewhat higher VCSEL area density. There are two qualitatively different VCSEL spacing regions shown in Fig. 7 by the dashed curve: spacing determined by the microlenses/superstrate, and spacing determined by the thermal limit (assumed to be 10 W/cm^2). VCSEL spacing determined by the thermal limit decreases with increasing VCSEL NA because in this case VCSELs are smaller, have lower threshold currents, and generate less heat; therefore more of them could be packed into the same chip area. VCSEL spacing determined by microlenses increases with increasing VCSEL NA. This is because large VCSEL NA requires microlenses to have larger diameters, which in turn causes VCSEL spacings to increase as VCSEL positions are now determined by the positions of nonoverlapping microlenses that collect the broadly divergent VCSEL beams.

These two curves cross at some value of VCSEL NA. The curve for VCSEL spacing incorporating both effects is shown as the dashed curve with a breakpoint at which the slope abruptly changes. The exact position of the breakpoint will depend on the assumptions made, but the general behavior will be given by a curve with shape similar to that of the dashed curve. Therefore, there is a "sweet spot" around the breakpoint on the dashed curve

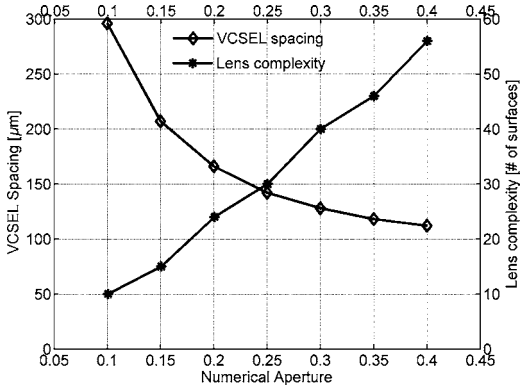

Fig. 6. VCSEL spacing and lens complexity as functions of VCSEL NA for the case *without* microlenses and with a thermal limit of 10 W/cm^2.

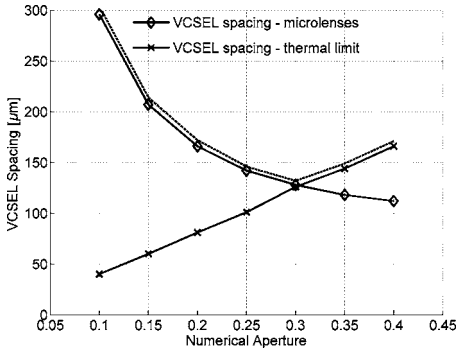

Fig. 7. VCSEL spacing and lens complexity as functions of VCSEL NA for the case *with* microlenses.

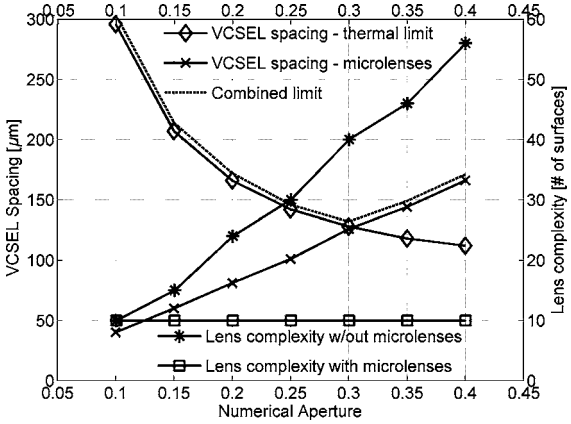

Fig. 8. VCSEL spacing and lens complexity as function of NA for the cases with and without microlenses.

that a good system design should exploit. The smallest and most efficient VCSELs may not be the best choice in FAST-Net systems—each case should be analyzed to determine the best operating point for a particular set of circumstances. For the analyzed case, this optimal NA is ~0.3.

It is possible to illustrate some further trade-offs in this system using Fig. 8, where graphs for VCSEL density and lens complexity are combined. If microlenses were used in the system (minimizing lens complexity), then the maximum VCSEL area density would be achieved by implementing VCSELs with NA close to the breakpoint value of the dashed curve. If microlenses were not used there would be no breakpoint in the dashed curve, and it would be possible to achieve better VCSEL area density by using higher beam divergence VCSELs, but a price would be paid in higher lens complexity. The optimal operating point for any specific system will be determined by the relative importance of minimizing the number of lens surfaces versus minimizing VCSEL spacing, i.e., by their respective relative cost functions.

It should be noted that an additional positive effect of using microlenses is that it decouples replacement efficiency from the VCSEL NA value, i.e., replacement efficiency parameter R stays at ~2, regardless of the fact that VCSELs have high NAs. This means not only that the number of lens surfaces is minimized but also that spherical surfaces can be efficiently replaced by aspherical surfaces and substantial savings made in lens volume, weight, and light loss.

The graphs that we present in Figs. 6–8 are valid for the superstrate thickness of 300 μm that was implemented in 2D VCSEL/photodetector arrays manufactured by Honeywell for the VIVACE system. Although the use of the superstrate for microlens support might appear to limit the generality of the analysis, in reality any other approach we are aware of implements some kind of support structure for either refractive or diffractive beam-shaping elements, with respective thicknesses in the hundreds of micrometers range.[25–28] Each of these structures would impose constraints similar to the one that implements the superstrate as microlens carrier, and they could be analyzed using this approach, too.

5. CONCLUSIONS

In this paper a framework for analyzing and minimizing optical complexity of free-space optically interconnected systems was developed. The approach was based on the disparity between VCSEL divergence angles and field of view of the optics. It was demonstrated that for the specific FSOI system analyzed the reduction in optical complexity was by a factor of ~2.

We also extended this approach and applied it to the analysis of density limitations of VCSEL arrays based on thermal and optical requirements. It was shown that use of microlenses to reduce VCSEL beam divergence could lower the complexity of optics but that it would also reduce VCSEL area density. We demonstrated the existence of an optimal VCSEL divergence if relative costs of optical complexity and device density were known.

ACKNOWLEDGMENTS

This work was supported by the Defense Advanced Research Projects Agency through the Air Force Wright Laboratory under contracts F33615-97-C-1054 and F33615-98-C-1356.

*Present address, Northrop Grumman Mission Systems, 5113 Leesburg Pike, Suite 400, Falls Church, Virginia 22041; e-mail, Predrag.Milojkovic@ngc.com.

REFERENCES AND NOTES

1. M. W. Haney, M. P. Christensen, P. Milojkovic, J. Ekman, P. Chandramani, R. Rozier, F. Kiamilev, L. Yue, and M. Hibbs-Brenner, "Multichip free-space global optical interconnection demonstration with integrated arrays of vertical-cavity surface-emitting lasers and photodetectors," Appl. Opt. **38**, 6190–6200 (1999).
2. M. W. Haney, M. P. Christensen, P. Milojkovic, G. J. Fokken, M. Vickberg, B. K. Gilbert, J. Rieve, J. Ekman, P. Chandramani, and F. Kiamilev, "Description and evaluation of the FAST-Net smart pixel-based optical interconnection prototype," Proc. IEEE **88**, 819–828 (2000).
3. M. W. Haney and M. P. Christensen, "Performance scaling comparison for free space optical and electrical interconnection approaches," Appl. Opt. **37**, 2886–2894 (1998).
4. R. R. Michael, M. P. Christensen, and M. W. Haney, "Experimental evaluation of the 3-D optical shuffle interconnection module of the sliding banyan network," J. Lightwave Technol. **9**, 1970–1978 (1996).
5. D. T. Nielson and C. P. Barrett, "Performance trade-offs for conventional lenses for free-space digital optics," Appl. Opt. **35**, 1240–1248 (1996).
6. A. G. Kirk, D. Plant, M. Ayliffe, M. Chateauneuf, and F. Lacroix, "Design rules for highly parallel free-space optical interconnects," IEEE J. Sel. Top. Quantum Electron. **9**, 531–547 (2003).
7. D. R. Rolston, B. Robertson, H. S. Hinton, and D. V. Plant, "Analysis of a microchannel interconnect based on the clustering of smart-pixel-device windows," Appl. Opt. **35**, 1220–1233 (1996).
8. G. Schulz, "Imaging performance of aspherics in comparison with spherical surfaces," Appl. Opt. **26**, 5118–5124 (1987).
9. G. Shulz, "Aberration-free imaging of large fields with thin pencils," Opt. Acta **32**, 1361–1371 (1985).
10. OSLO SIX, Sinclair Optics, 6780 Palmyra Road, Fairport, New York 14450.
11. P. Milojkovic, M. P. Christensen, and M. W. Haney, "Minimum lens complexity design approach for a free-space macro-optical multi-chip global interconnection module," presented at the Optics in Computing 2000 Conference, Quebec City, Canada, June 18–23, 2000.
12. T. E. Sale, *Vertical Cavity Surface Emitting Lasers* (Wiley, 1995), pp. 23, 24.
13. E. Towe, ed., *Heterogeneous Optical Integration* (SPIE, 2000), Chap. 4.
14. M. Christensen, P. Milojkovic, and M. W. Haney, "Multiscale optical design for global chip-to-chip optical interconnections and misalignment tolerant packaging," IEEE J. Sel. Top. Quantum Electron. **9**, 548–556 (2003).
15. C. Gimkiewicz and J. Jahns, "Air cooling of a VCSEL diode array on quartz," 1998, http://www.fernuni-hagen.de/ONT/Forschungsinhalt/jb98/CG3.pdf.
16. C. Gimkiewicz, G. Grabosch, D. Hagedorn, and J. Jahns, "Cooling of laser diode arrays in planar optical systems," 2000, http://www.fernuni-hagen.de/ONT/Forschungsinhalt/jb00/Cooling.pdf.
17. M. Miller and I. Kardosh, "Improved output performance of high-power VCSELs," *Annual Report 2001*, Optoelectronics

Department, University of Ulm, www.opto.e-technik.uni-ulm.de/forschung/jahresbericht/2001/ar01mim.pdf.
18. D. Francis, H. L. Chen, W. Yuen, G. Li, and C. Chang-Hasnain, "Monolithic 2-D VCSEL array with >2 W CW and >5 W pulsed power," Electron. Lett. **34**, 2132–2133 (1998).
19. Y. Liu, "Heterogeneous integration of optoelectronic element arrays with Si electronics and micro-optics," IEEE Trans. Adv. Packag. **25**, 43–49 (2002).
20. K. L. Lear, R. P. Schneider, Jr., K. D. Choquette, and S. P. Kilcoyne, "Index guiding dependent effects in implant and oxide confined vertical-cavity lasers," IEEE Photon. Technol. Lett. **8**, 740–742 (1996).
21. J. Lehman, "Honeywell advanced photonics development overview," presented at the 2nd Workshop on Optical Read-out Technologies for ATLAS Oxford, UK, January 7, 1999; www.cern.ch/Atlas/GROUPS/FRONTEND/links/oxford_wkshp/honeywell.ppt.
22. C. Wilmsen, H. Temkin, and L. Coldren, eds. *Vertical-Cavity Surface-Emitting Lasers* (Cambridge U. Press, 1999), p. 222.
23. This is not taken directly from any particular VCSEL data sheet (it is just a convenient starting point for calculations), but there are a number of VCSEL products that have specs that approximately match this assumption. For example, see http://www.ulm-photonics.de/docs/pdfs/17032003/VCSEL-ULM-5G-1x1-chip.pdf.
24. J. Eckman and X. Wang, University of Delaware, private communication (January 2004).
25. L. A. Coldren, Y. A. Akulova, E. M. Strzelecka, B. J. Thibeault, J. C. Ko, and D. A. Louderback, "VCSEL array packaging for free space interconnects," Report 1996-97 for MICRO Project 96-050, UCSB Santa Barbara Research Center.
26. Yongqi Fu and Ngoi Kok Ann Bryan, "Investigation of hybrid microlens integration with vertical cavity surface-emitting lasers for free-space optical links," Opt. Express **10**, 413–418 (2002).
27. S. Eitel, S. J. Fancey, H. P. Gauggel, K. H. Gulden, W. Baechtold, and M. R. Taghizadeh, "Highly uniform vertical-cavity surface-emitting lasers integrated with microlens arrays," IEEE Photon. Technol. Lett. **12**, 459–461 (2000).
28. Yongqi Fu, "Integration of microdiffractive lens with continuous relief with vertical-cavity surface-emitting lasers using focused ion beam direct milling," IEEE Photon. Technol. Lett. **13**, 424–426 (2001).